Journal of Power Sources 248 (2014) 570–576

Contents lists available at ScienceDirect

Journal of Power Sources

journal homepage: www.elsevier.com/locate/jpowsour

Multi-walled carbon nanotubes @ mesoporous carbon hybrid nanocomposites from carbonized multi-walled carbon nanotubes @ metal–organic framework for lithium sulfur battery

Weizhai Bao [a], Zhian Zhang [a,b,*], Chengkun Zhou [a], Yanqing Lai [a,b], Jie Li [a,b]

[a] School of Metallurgy and Environment, Central South University, Changsha, Hunan 410083, China
[b] Engineering Research Center of High Performance Battery Materials and Devices, Research Institute of Central South University in Shenzhen, Shenzhen 518057, China

HIGHLIGHTS

- A novel design and synthesis of MWCNT@Meso-C using MWCNT@MOF-5 as precursor.
- MWCNT@Meso-C hybrid material as a host material was applied for sulfur cathode.
- Electrochemical performances were improved in sulfur cathode using MWCNT@Meso-C.

ARTICLE INFO

Article history:
Received 27 August 2013
Received in revised form
26 September 2013
Accepted 30 September 2013
Available online 6 October 2013

Keywords:
Lithium sulfur battery
Sulfur cathode
Multi-walled carbon nanotubes
Carbonization

ABSTRACT

We present a design and synthesis of a hierarchical architecture of multi-walled carbon nanotubes @ mesoporous carbon (MWCNT@Meso-C) using unique multi-walled carbon nanotubes @ metal–organic framework (MWCNT@MOF-5) as both template and precursor. Active sulfur is encapsulated into the MWCNT@Meso-C matrix prepared via carbonizing MWCNT@MOF-5 polyhedrons for high performance lithium sulfur battery. The initial and 50th cycle discharge capacity of MWCNT@Meso-C/S sulfur cathode are as high as 1343 mAh g^{-1} and 540 mAh g^{-1} at a high current rate of 0.5 C. CV and EIS tests indicate that the MWCNT@Meso-C/S sulfur cathode has smaller resistance and better kinetics characteristics than that of the MWCNT@MOF-5 sulfur cathode. Test results indicate that the MWCNT@Meso-C is a promising host material for the sulfur cathode in the lithium sulfur battery applications.

1. Introduction

With the rapid development of portable electronic equipment, electric vehicles and intelligent power grid and other areas, a higher demand for batteries with high power and energy density and longer cycling life has been put forward, therefore developing a new generation of battery system is becoming more and more urgent [1]. Lithium sulfur batteries have been studied as one of the most promising systems for the next generation high-energy rechargeable lithium batteries because of their high theoretical specific capacity (~1680 mAh g^{-1}) and energy density (2600 Wh kg^{-1}) [2]. However, the poor electrical conductivity of elemental sulfur and the fast-capacity degradation from polysulfide dissolution into the electrolyte have greatly limited its practical applications [3,4].

Past research efforts have been devoted to address these issues such as optimization of the electrolyte, replacing binder [5,6]. Besides, several approaches were pursued to prepare highly electronic conducting, porous carbon/sulfur composites in order to capture polysulfide species within the electrode configuration [7–9]. For instance, Huang et al. proposed a new composite structure of graphene–sulfur with a high electrochemical performance [7]. In particular, porous carbon materials have attracted intensive attention due to their good compatibility with sulfur, easy accessibility, and the abundance of candidates with diverse porosity and structure. Among the most elegant ones is Nazar's approach which relies on the use of ordered mesoporous carbon composite so as to provide both an electronic percolation path through the electrode and an adequate controlled porosity to retain part of the

* Corresponding author. School of Metallurgy and Environment, Central South University, Changsha, Hunan 410083, China. Tel./fax: +86 731 88830649.
E-mail address: zza75@163.com (Z. Zhang).

0378-7753/$ – see front matter © 2013 Elsevier B.V. All rights reserved.
http://dx.doi.org/10.1016/j.jpowsour.2013.09.132

electrochemically generated polysulfides species. Zhang et al. reported that sulfur was encapsulated in the mesoporous carbon foams (MCF) framework which succeeded in efficiently trapping sulfur in the MCF host and achieved a high utilization of active sulfur mass [8,9].

To the best of our knowledge, metal–organic frameworks (MOFs) have even richer pore structure and larger specific surface area than the nano-structured porous carbon [10]. Depending on the metal and organic-ligand selected, networks with various pore shape, size, volume, chemistry can be synthesized and thus adapted to the specific needs of lithium–sulfur battery. Recently, there has been growing research interest for the application of metal organic framework in lithium sulfur battery. Tarascon et al. presented a strategy based on the use of a metal organic framework (MOF) as host material for sulfur cathode [11]. However, due to the poor conductivity of the MOFs and sulfur particle themselves, the sulfur cathode has to add a large amount of conductive carbon in order to ensure the normal charge and discharge of the lithium sulfur battery. To solve these problems, Kumar et al. proposed a method of carbonized MOFs for sulfur loading to fabricate cathode structures for lithium sulfur batteries [12]. Zhang et al. synthesized a porous carbon via pyrolysis of MOF using in lithium sulfur battery [13]. The porous carbon derived from MOFs without any modification exhibits uniform porosity and porous structure. However, the electronic conductivity of porous carbon derived from MOFs without any modification is much lower than that of other graphite based materials [14]. The poor electronic conductivity of porous carbon severely limits the electrochemical performance of mesoporous carbon/sulfur composite, especially in a high current rate.

Multi-walled carbon nanotubes (MWCNTs) have been used as carbon matrix and electric conductor for sulfur cathodes because of their high conductivity and unique structure in addition to the high aspect ratio of MWCNTs, providing faster Li^+ diffusion pathways. It has been reported that the cyclability of lithium–sulfur battery can be improved by combining sulfur with MWCNTs [14]. Inspired by these previous studies, we demonstrate combining the advantages of multi-walled carbon nanotubes (MWCNTs) and mesoporous carbon (Meso-C) materials to yield the hierarchical architecture of multi-walled carbon nanotubes and mesoporous carbon (MWCNT@Meso-C) hybrid nanocomposites with both uniform porosity and good electronic conductivity, which might serve as a high performance matrix for lithium sulfur battery.

Here we report a rational design and synthesis of a hierarchical architecture of multi-walled carbon nanotubes @ mesoporous carbon (MWCNT@Meso-C) using unique multi-walled carbon nanotubes @ metal–organic framework hybrid materials (MWCNT@MOF-5) as both template and precursor. Active sulfur is encapsulated into the MWCNT@Meso-C matrix prepared via carbonizing MWCNT@MOF-5 material for high performance lithium–sulfur battery. Carbonizing MWCNT@MOF-5 material proposes a new preparation method for hybrid material. MWCNT@Meso-C/S sulfur cathode shows an obviously improved electrochemical performance, including better cycle performance, higher discharge capacity, smaller resistance and better kinetics characteristics. These results show that MWCNT@Meso-C hybrid material is a promising host material for the sulfur cathode in the lithium sulfur battery applications.

2. Experimental

2.1. Preparation of MWCNT@Meso-C/sulfur multi-composites (MWCNT@Meso-C/S)

MWCNTs (Shenzhen Nanotech., China.) were soaked in mixed acid (a mixture of nitric acid and sulfuric acid) for 24 h at 80 °C with stirring, recovered by filtration, washed with deionized water, and dried at 70 °C. Twenty milligrams of MWCNTs were dispersed in 20 mL of DMF. MWCNT@Meso-C was prepared from one-step pyrolysis of MOF-5@MWCNT, which was obtained via simple solvothermal reaction. Typically, MWCNTs/DMF (10 mg/10 mL) was mixed with 30 mL of DMF containing predissolved zincnitrate hexahydrate (0.178 g, 0.6 mmol) and terephthalic acid (0.033 g, 0.2 mmol). The resulting mixture was vigorously stirred for 2 h at room temperature. The mixture was heated to 105 °C in a furnace and maintained at that temperature for 24 h without stirring. The reaction vessel was then removed from the furnace and allowed to cool to room temperature. The crystals were repeatedly washed with DMF, filtered and vacuum-dried under 10^{-3} Torr at 150 °C for 24 h [15,16]. The as-prepared MWCNT@MOF-5 was transferred to a tube furnace and was heat-treated at 900 °C for 3 h under nitrogen with a heating rate of 5 °C min^{-1} to pyrolyze the organic species [17,18]. Then the material was cooled to room temperature and MWCNT@Meso-C was obtained. To prepare the MWCNT@Meso-C/S composite, the mixture of MWCNT@Meso-C and element sulfur was heated at 155 °C in Ar atmosphere for 20 h. According to thermogravimetric analysis (TGA), MWCNT@Meso-C/S multi-composites have 58.27 wt% sulfur content. For comparison, MWCNT@MOF-5/S composite was prepared by the same procedure (sulfur content 58.14 wt%).

2.2. Electrode preparation

The cathode slurry was prepared by mixing 80 wt% MWCNT@Meso-C/S multi-composites, 10 wt% carbon black (Super P, Timcal) and 10 wt% PVDF (6020, Solef). For comparison, the slurry using MWCNT@MOF-5/S composite was prepared by a similar route. Then, the slurry was spread onto aluminum foil current collector (20 μm thickness) by a doctor blade. The electrode was dried under vacuum at 60 °C for 24 h. The sulfur loading density of the cathode was 1.5 mg cm^{-2}, and the total thickness of electrode layer was approximately 30 μm. MWCNT@Meso-C/S cathode and MWCNT@MOF-5/S cathode were obtained using MWCNT@Meso-C/sulfur and MWCNT@MOF-5/sulfur, respectively.

2.3. Cell assembly and characterization

Coin-type (CR2025) cells were assembled in an argon-filled glove box (Universal 2440/750) in which oxygen and water contents were less than 1 ppm. Sulfur-containing electrode was used as the cathode, lithium foil as the counter and reference electrode, microporous polypropylene membrane as the separator, and 1.5 mol L^{-1} lithium bis(trifluoromethane sulfonyl)imide (LiTFSI, 99.95%, Aldrich) in a solvent mixture of 1,3-dioxolane and 1,2-dimethoxyethane (1:1, v/v) as the electrolyte.

Cyclic voltammetry (CV) and electrochemical impedance spectroscopy measurements were conducted using Solartron 1470E cell test. CV tests were performed at a scan rate of 0.2 mV s^{-1} in the voltage range from 1.5 to 3.0 V. The galvanostatic charge/discharge tests were carried out in the potential range from 1.5 to 3.0 V under a LAND CT2001A charge–discharge system. All experiments were conducted at room temperature.

The morphologies analyses were observed with a scanning electron microscopy (FEI Quanta-200) and a Hitachi H-700 transmission electron microscopy (TEM) (Tecnai G220ST). X-ray diffraction (XRD) (Rigaku3014) measurements were made with Cu Kα radiation. The structure of the samples was tested by Raman spectrometer (Jobin-Yvon LabRAM HR-800, Horiba).

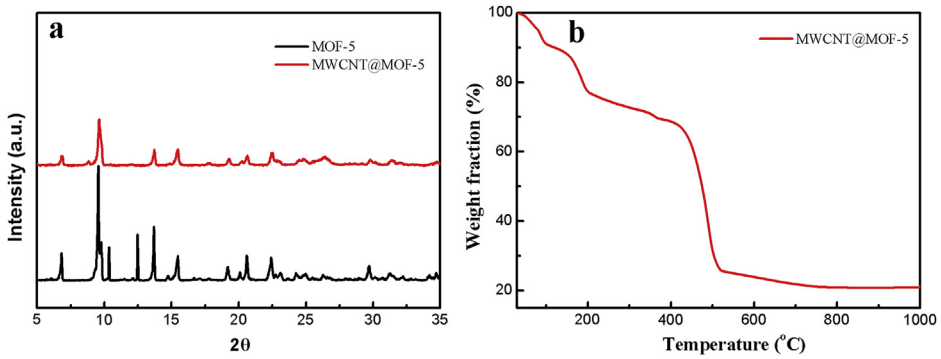

Fig. 1. XRD pattern of the MOF-5 and MWCNT@MOF-5 (a), TGA curve of MWCNT@Meso-C from the pyrolysis of MWCNT@MOF-5 (b).

3. Results and discussion

3.1. Materials characterization

To identify lattice structure of MOF-5 and the as-prepared MWCNT@MOF-5 sample, XRD was employed. Fig. 1 illustrates the XRD pattern of the MOF-5 and MWCNT@MOF-5 sample. XRD pattern reveal the crystal structure MOF-5 and the MWCNT@MOF-5 hybrid composite clearly. Crystal faces for all the peaks are also identified based on the crystallographic data. XRD patterns of virgin MOF-5 and MWCNT@MOF-5 are found to be in perfect agreement with earlier data on MOF-5 [19], confirming the successful synthesis of MOF-5 and MWCNT@MOF-5. Furthermore, the characteristic peaks of MWCNT@MOF-5 matched well with that of MOF-5. The characteristic MWCNTs peak, normally at 26–27°, is swamped by high-intensity MOF-5 peaks. Thus, we can speculate that MWCNT incorporation did not disturb or destroy the MOF-5 crystal structure.

In order to describe main structural changes in the MWCNT@MOF-5 during carbonization clearly, TGA measurement under a N_2 atmosphere was carried out to investigate the carbonization process of MWCNT@MOF-5. As displayed in Fig. 1b, the mass loss during the temperature region of 200–400 °C is attributed with the evaporation of solvents (DMF) remaining in the pores of MOF-5. The next mass loss is mainly due to the decomposition of the ligand molecules during 450–550 °C. After above carbonization, the composites are composed of ZnO and carbonaceous materials. When the temperature attains 600–900 °C, the change of the TG curve is accompanied by the evaporation of CO_2, CO and slight amounts of ZnO and Zn. This transition corresponds to the reduction of ZnO to Zn and the oxidation of a carbonaceous material to form mainly CO and CO_2. The reduced Zn metal is easily vaporized with heating at 900 °C and the mass of the remainer does not change after 900 °C. In summary, the TG curve consists of three apparent stages of mass loss, which agrees well with the result of the previous literature [17,18]. The conjugate of carbonaceous materials is easily obtained after the high temperature of carbonization. MWCNT@Meso-C and sulfur are both hydrophobic so that they have better compatibility at 155 °C. The developed porous structure is favorable for the diffusion of melt sulfur and the access connection of the electrolyte, which agrees well with the result of the XRD images (Fig. 2b).

Raman spectra of Meso-C and MWCNT@Meso-C was carried out to observe their carbon structure and surface defect (Fig. 2a). All spectra were excited with visible (640 nm) laser light. We did not observe obvious peak shifts of the MOF bands in Raman except for the appearance of bands associated with graphite, confirming the successful carbonization process. The main features in the Raman of Meso-C and MWCNT@Meso-C are the so-called D (1351) and G (1572) bands, which are known as the disorder induced and in-plane E2 g zone center modes, respectively [20]. Furthermore, the Raman band at around 2500–2750 is used widely as an indicator of high quality of grapheme, proving the existence of MWCNTs in the MWCNT@Meso-C. This result is consistent with the reported of the literature [20]. This result proved the successful carbonization process from MWCNT@MOF-5 to MWCNT@Meso-C [18]. Fig. 2b illustrates the XRD pattern of the Meso-C, MWCNT@Meso-C, MWCNT@Meso-C/S composites, MWCNT@Meso-C/S mixed and sulfur sample. The XRD patterns for the Meso-C, MWCNT@Meso-C samples were found to be in agreement with earlier data on porous carbon [9]. Furthermore, compared with the pattern of Meso-C, the characteristic MWCNT peak in the XRD pattern of MWCNT@Meso-

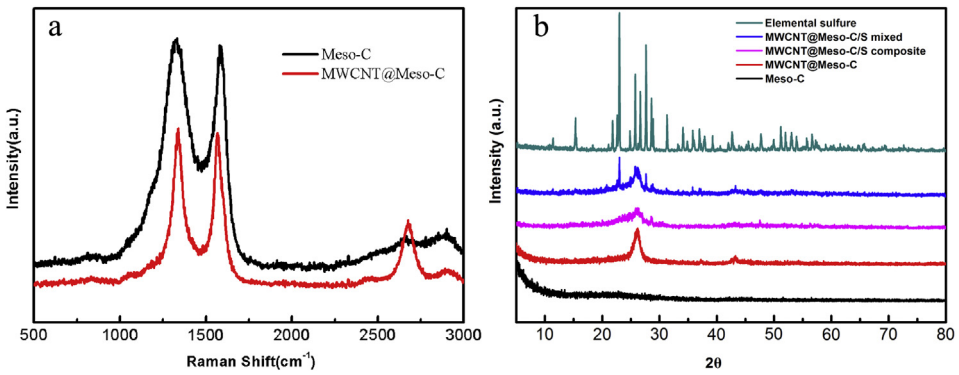

Fig. 2. Raman spectra of Meso-C and MWCNT@Meso-C (a), XRD pattern of the Meso-C, MWCNT@Meso-C, MWCNT@Meso-C/S composite, MWCNT@Meso-C/S mixed and sulfur sample (b).

C composites, normally at 26–27° is easily detectable [20]. These experimental results reveal that the definite existence of MWCNTs in the MWCNT@MOF-5 crystallites and MWCNT@Meso-C matrix.

To further understand the composition and structure of the MWCNT@Meso-C/S composite, X-ray diffraction (XRD) was used. Fig. 2b shows the characteristic XRD pattern of the simple mixture of MWCNT@Meso-C/sulfur powder, the as-prepared MWCNT@Meso-C/S composite and elemental sulfur, respectively. Compared with the pattern of the simple mixture of MWCNT@Meso-C/sulfur powder (MWCNT@Meso-C/S mixed), the characteristic sulfur peaks in the XRD pattern of MWCNT@Meso-C/S composite are not easily detectable, corresponding to bulk crystalline sulfur completely disappear after sulfur impregnation. This result indicates the sublimed sulfur is amorphous or that the sulfur particles trapped in the MWCNT@Meso-C carbon matrix are unable to crystallize [9,21].

The scanning electron microscopy (SEM) and transmission electron microscopy (TEM) analysis were used to investigate the microstructure of the as-synthesized samples. SEM images of MOF-5, Meso-C, MWCNT@MOF-5, MWCNT@Meso-C, MWCNT@Meso-C/S multi-composites were given (Fig. 3a–e). Fig. 3a, c is the SEM images of MOF-5, MWCNT@MOF-5. The morphology of MOF-5 and MWCNT@MOF-5 were characterized by well-defined cubic crystals 50–150 μm in width. These images further identify crystal size and lattice structure of the as-prepared MOF-5, which match well with the structure reported in the literature [15,16] and agrees well with the result of the XRD images (Fig. 1a), confirming that the successful synthesis of MOF-5 and MWCNT@MOF-5. The porous morphology of mesoporous carbon (Meso-C) derived from pyrolysis of metal–organic framework (MOF-5) is shown in Fig. 3b. Meso-C consists of carbon matrix with a wealth of pore structure. Fig. 3d presents the SEM images

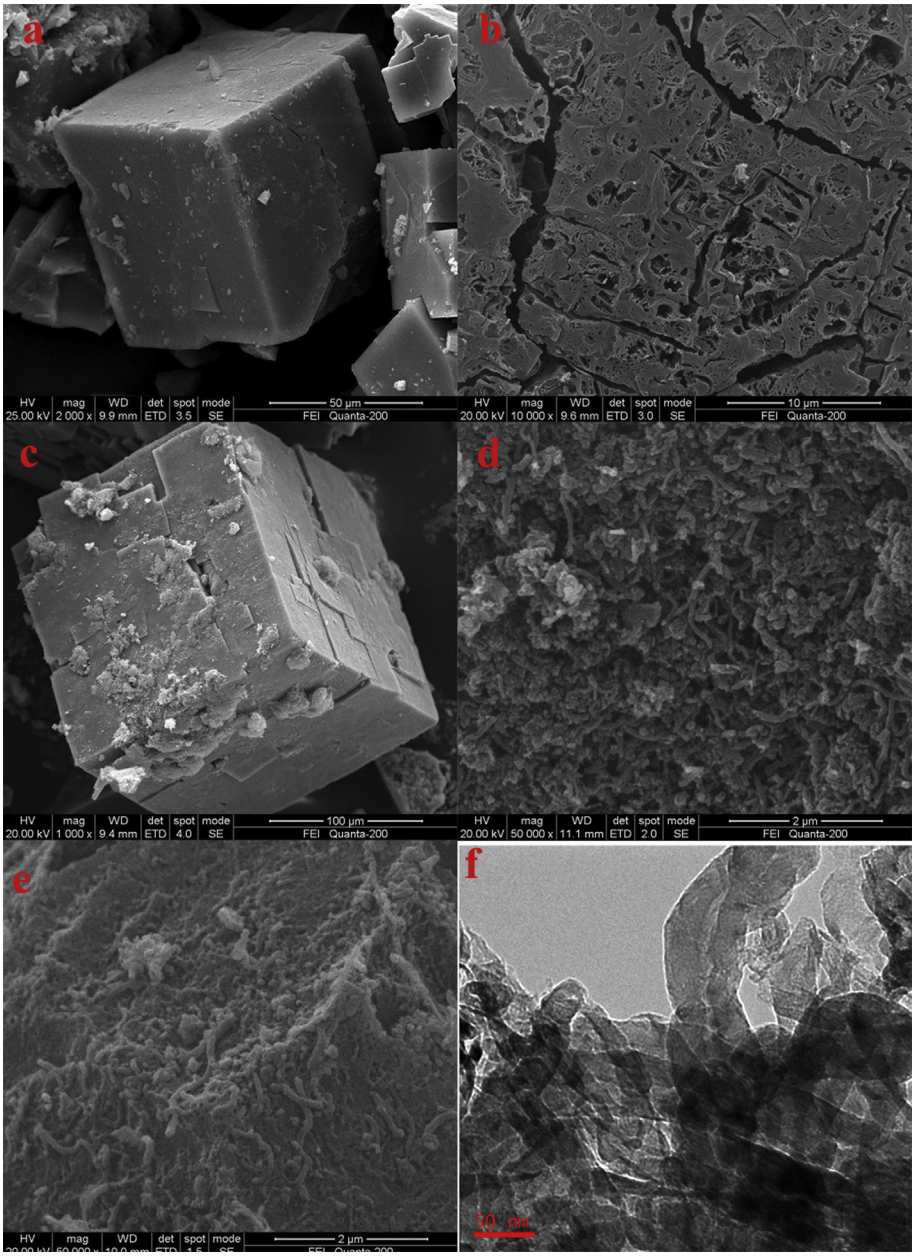

Fig. 3. SEM images of MOF-5 (a), Meso-C (b), MWCNT@MOF-5 (c), MWCNT@Meso-C (d), MWCNT@Meso-C/S multi-composite (e), TEM images of MWCNT@Meso-C (f).

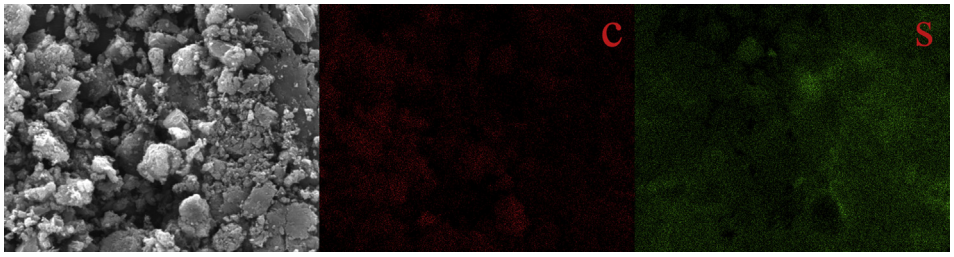

Fig. 4. The corresponding elemental mapping of S, C for MWCNT@Meso-C/S multi-composite.

of MWCNT@Meso-C, microstructure images derived from pyrolysis of MWCNT@MOF-5. Compared with the SEM images in Fig. 3b, d reveals that MWCNTs are uniformly distributed and embedded in the space framework of Meso-C. The hybrid composite shows combined morphology consisting of MWCNT and Meso-C, which agrees well with the result of the TEM images (Fig. 3f), confirming that the successful carbonization process from MWCNT@MOF-5 to MWCNT@Meso-C and MWCNT were indeed uniformly dispersed in the MWCNT@Meso-C matrix successfully. Furthermore, the experimental results reflects that MWCNTs are indeed well admixed with MOF-5 crystallites and the successful synthesis of MWCNT@MOF-5 from the other side. In summary, the SEM and TEM images in Fig. 3d, f shows MWCNT are indeed uniformly dispersed in the MWCNT@Meso-C matrix successfully, thereby MWCNT@Meso-C hybrid nanocomposites can provide a conductive network and faster Li^+ diffusion pathways for the cathode, which could effectively improve the conductive properties of the composite material and favor the transportation of ions during cycling. SEM image of the as-prepared MWCNT@Meso-C/S composite is shown in Fig. 3e. Compared with Fig. 3d, e shows that a large portion of the porosity within MWCNT@Meso-C was filled with sulfur, suggesting the full incorporation of sulfur into carbon matrix of MWCNT@Meso-C during the heat treatment process.

Furthermore, in order to characterize the dispersion of the sulfur particles in the composite material clearer, the corresponding elemental mapping of S and C within the MWCNT@Meso-C/S composite are respectively shown in Fig. 4 The S elemental mapping clearly demonstrates that no discernible sulfur particles can be found outside of the MWCNT@Meso-C particles and sulfur is homogeneously distributed within the carbon matrix of MWCNT@Meso-C, which agrees well with the result of the XRD images (Fig. 2b) and the SEM images (Fig. 3e).

3.2. Electrochemical characterization

In order to demonstrate the advantageous electrochemical properties of the MWCNT@Meso-C/S sulfur cathode, cycle performance of MWCNT@Meso-C/S sulfur cathode and MWCNT@MOF-5/S sulfur cathode between the 1.5 V–3.0 V voltage limits at the current density of 837.5 mA g^{-1} (0.5 C) are exhibited in Fig. 5a. It can be seen that the capacity of both the sulfur cathodes decrease with an increased number of cycles. The discharge capacity of MWCNT@MOF-5/S sulfur cathode is 874 mAh g^{-1} for the initial cycle and decrease to 272 mAh g^{-1} after 50 cycles, which is similar with the result reported of previous literature [11–13]. Whereas the discharge capacity of MWCNT@Meso-C/S sulfur cathode is 1343 mAh g^{-1} for the initial cycle and a high reversible capacity of 540 mAh g^{-1} is retained after 50 cycles, showing a great improvement in cyclability, especially relatively higher special capacity and higher capacity retention rate. MWCNT @Meso-C hybrid nanocomposites provide a conductive network and faster Li^+ diffusion pathways for the cathode, which could effectively improve the conductive properties of the composite material and is beneficial to the high discharge capability of the sulfur cathode. At the same time, the mesopores matrix of MWCNT@Meso-C essentially slows down the polysulfides diffusivity out of the pore during cycling due to such a strong adsorption, avoiding the shuttle reaction. Therefore, even at the current density of 837.5 mA g^{-1} (0.5 C), MWCNT@Meso-C/S sulfur cathode can show a remarkably higher special capacity than the MWCNT@MOF-5/S sulfur cathode, which is better than the previous report [11–13]. At the same time, we find that capacity fade of MWCNT@Meso-C/S sulfur cathode seems slightly quick compared to MWCNT@MOF-5/S composite sulfur cathode after 10 cycles in Fig. 5. After carefully checking the relevant literature, similar experimental result was found in the following literature

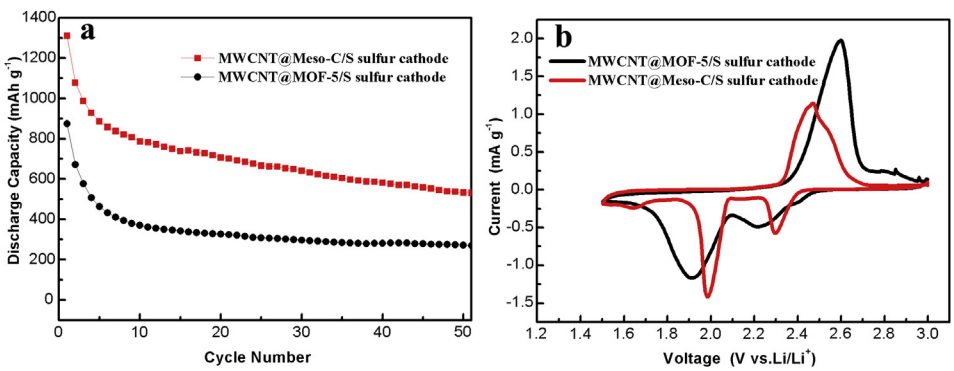

Fig. 5. Cycle performance of the MWCNT@Meso-C/S composite sulfur cathode and MWCNT@MOF-5/S composite sulfur cathode at 0.5 C (a), cyclic voltammogram curves of the Li/S cells with the MWCNT@Meso-C/S composite sulfur cathode and the MWCNT@MOF-5/S composite sulfur cathode at a scan rate of 0.2 mV s^{-1} (b).

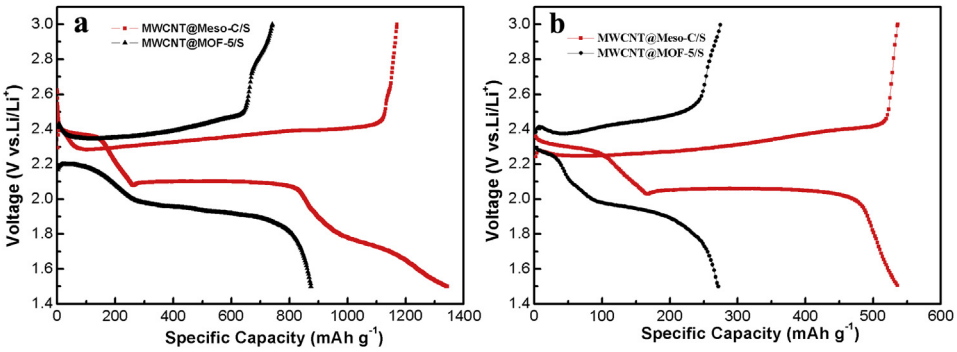

Fig. 6. Discharge/charge curves of MWCNT@Meso-C/S composite sulfur cathode and MWCNT@MOF-5/S composite sulfur cathode at 0.5 C at the initial cycle (a) and 50th cycle (b).

[1–3]. It may be the differences in pore structure between MWCNT@MOF-5 and MWCNT@Meso-C led to the above mentioned experimental results [12,22].

Cyclic voltammogram curves of the Li/S cells with the 1st cycle of MWCNT@Meso-C/S and MWCNT@MOF-5/S sulfur cathode at a scan rate of 0.1 mV s^{-1} are shown in Fig. 5b. The curves in Fig. 5b shows two distinct reduction peaks and one oxidation peak. Two pronounced reduction peaks around 2.0 V and 2.3 V, and the only one sharp oxidation peak observed at the potential of 2.5 V in the anodic scan, is corresponding to the conversion of lithium sulfide into high-order polysulfides [23]. Furthermore, the reduction and oxidation peaks of the MWCNT@Meso-C/S cathode appear much sharper than those of the MWCNT@MOF-5/S cathode, and the voltage difference (ΔE) between oxidation and reduction peaks for MWCNT@Meso-C/S cathode is also smaller. This illustrates that the MWCNT@Meso-C/S sulfur cathode has better kinetics characteristics. Considering that the ΔE is determined by the potential polarization of the active material during the charge and discharge process, the lower ΔE and the sharper peak also indicates an improvement of conductivity and electrochemical reversibility of the cell with cycling in the MWCNT@Meso-C/S cathode system.

Galvanostatic charge/discharge tests were carried out at a relatively high current density of 837.5 mA g^{-1} (0.5 C). The charge/discharge curves of Li/S cells using MWCNT@Meso-C/S sulfur cathode and MWCNT@MOF-5/S sulfur cathode at 1st cycle and 50th cycle are shown in Fig. 6b. Both the discharge curves of the sulfur cathodes display two typical discharge potential plateaus, corresponding to the multistep of reduction reaction of sulfur during the discharge process, similar to the case reported by Choi [23]. The high plateau (around at 2.3 V) is caused by the changes from element sulfur to higher-order lithium polysulfides (Li_2S_n, $4 \leq n \leq 8$) while the predominantly low plateau (around at 2.0 V) is related to the reduction of higher-order polysulfides to lower-order polysulfides (Li_2S_2 or Li_2S) [24]. As seen, MWCNT@Meso-C/S sulfur cathode shows lower charge plateau potential and higher discharge plateau potential than that of MWCNT@MOF-5/S sulfur cathode. The smaller potential separation between the charge and discharge plateaus indicates better kinetics characteristics of MWCNT@Meso-C/S sulfur cathode consistent with the results of CV (Fig. 5b).

To understand the improved electrochemical performance of the MWCNT@Meso-C/S composite, Fig. 7 presents the electrochemical impedance spectroscopy (EIS) analysis of MWCNT@Meso-C/S and MWCNT@MOF-5/S sulfur cathode before the first discharge and after 50 cycles respectively. For the cathodes before the first discharge, as shown in Fig. 7a, the impedance plots are composed of a depressed semicircle at high frequency, and an inclined line at low frequency. The semicircle corresponds to the internal resistance of the cathode including bulk impedance and interfacial impedance. In addition, the inclined line at low frequency reflects the Li ion diffusion into the active mass. It can be seen in Fig. 7a that the internal resistance of MWCNT@Meso-C/S cathode are smaller than that of MWCNT@MOF-5/S sulfur cathode. As shown in Fig. 7b, the impedance plots of the cathodes after 50 cycles are composed of two depressed semicircles at high frequency and middle frequency, respectively, and an inclined line at low frequency. The semicircle in high frequency region corresponds to the resistance of solid-state layer of accumulated lithium sulfide, and the semicircle at middle frequency is considered as the charge transfer resistance. In addition, the inclined line at low frequency reflects the Li ion diffusion into the active mass. It can be clearly seen in Fig. 7 that charge transfer resistance of MWCNT@Meso-C/S sulfur cathode are

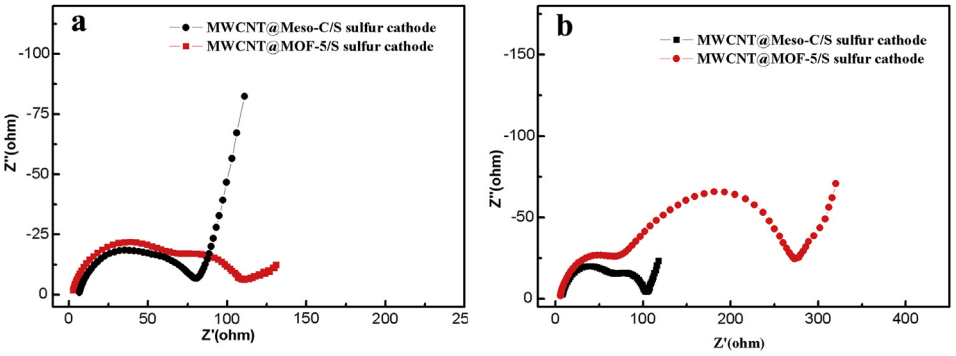

Fig. 7. Nyquist plots for the Li/S cells with MWCNT@Meso-C/S composite sulfur cathode and MWCNT@MOF-5/S composite sulfur cathode: (a) before cycling and (b) after 50th cycle.

much smaller than that of MWCNT@MOF-5/S sulfur cathode showing the remarkable electrochemical performance of the MWCNT@Meso-C/S composite. It can be concluded that MWCNT@Meso-C/S sulfur cathode shows a smaller resistance consistent with the results of CV (Fig. 5b). It suggests that the MWCNT@Meso-C/S sulfur cathode is favorable to improve electrochemical performance of lithium sulfur battery.

4. Conclusions

In this paper, we report a rational design and synthesis of a hierarchical architecture MWCNT@Meso-C using unique MOF-5@MWCNT polyhedrons as both template and precursor. Active sulfur is encapsulated into MWCNT@Meso-C matrix prepared via carbonizing MWCNT@MOF-5 material for high performance lithium–sulfur battery. Carbonizing MOF-5@MWCNT polyhedrons proposes a new preparation method of hybrid nanocomposites material. The initial and 50th cycle discharge capacity of MWCNT@Meso-C/S sulfur cathode are as high as 1343 mAh g^{-1} and 540 mAh g^{-1} at a high current rate of 0.5 C, respectively. MWCNT@Meso-C/S sulfur cathode has smaller resistance and better kinetics characteristics than that of the MWCNT@MOF-5 sulfur cathode Test results indicate that the MWCNT@Meso-C composite is a promising host material for the sulfur cathode in the lithium sulfur battery applications.

Acknowledgments

The authors thank the financial support of the Strategic Emerging Industries Program of Shenzhen, China (JCYJ201206 18164543322) and National Natural Science Foundation of China (20803095). We also thank the support of the Engineering Research Center of Advanced Battery Materials, the Ministry of Education, China.

References

[1] A. Manthiram, Y. Fu, Y.S. Su, Acc. Chem. Res. 45 (2013) 1125–1134.
[2] R.V. Noorden, Nature 498 (2013) 416–417.
[3] Z.W. Seh, W.Y. Li, J.J. Cha, G.Y. Zheng, Y. Yang, M.T. McDowell, P.C. Hsu, Y. Cui, Nat. Commun. 4 (2013) 1331.
[4] E.S. Shin, K. Kim, S.H. Oh, W.I. Cho, Chem. Commun. 49 (2013) 2004–2006.
[5] S.S. Zhang, J. Power Sources 231 (2013) 153–162.
[6] Z.A. Zhang, W.Z. Bao, H. Lu, M. Jia, K.Y. Xie, Y.Q. Lai, J. Li, ECS Electrochem. Lett. 1 (2012) A34–A37.
[7] T.Q. Lin, Y.F. Tang, Y.M. Wang, H. Bi, Z.Q. Liu, F.Q. Huang, X.M. Xie, M.H. Jiang, Energy Environ. Sci. 6 (2013) 1283–1290.
[8] X.Y. Tao, X.R. Chen, Y. Xia, H. Huang, Y.P. Gan, R. Wu, F. Chen, W.K. Zhang, J. Mater. Chem. A 1 (2013) 3295–3301.
[9] X. Ji, K.T. Lee, L.F. Nazar, Nat. Mater. 8 (2009) 500.
[10] L.F. Song, J. Zhang, L.X. Sun, F. Xu, F. L, H.Z. Zhang, X.L. Si, H.Y. Zhou, D.L. Sun, Y. Du, Z. Cao, Z. Gabelica, Energy Environ. Sci. 5 (2012) 7508–7520.
[11] R.D. Cakan, M. Morcrette, F. Nouar, C. Davoisne, T. Devic, D. Gonbeau, R. Dominko, C. Serre, G. Ferey, J.M. Tarascon, J. Am. Chem. Soc. 133 (2011) 16154–16160.
[12] K. Xi, S. Cao, X.Y. Peng, C. Ducati, R.V. Kumar, A.K. Cheetham, Chem. Commun. 49 (2013) 2192–2194.
[13] G.Y. Xu, B. Ding, L.F. Shen, P. Nie, J.P. Han, X.G. Zhang, J. Mater. Chem. A 1 (2013) 4490–4496.
[14] D.L. Wang, Y.C. Yu, W.D. Zhou, H. Chen, F.J. DiSalvo, A.M. Hector, D. Abrun, Phys. Chem. Chem. Phys. 15 (2013) 9051–9057.
[15] S.J. Yang, J.Y. Choi, H.K. Chae, J.H. Cho, K.S. Nahm, C.R. Park, Chem. Mater. 21 (2009) 1893–1897.
[16] Z.H. Xiang, X. Peng, X. Cheng, X.J. Li, D.P. Cao, J. Phys. Chem. C 115 (2011) 19864–19871.
[17] W. Chaikittisilp, K. Arig, Y. Yamauchi, J. Mater. Chem. A 1 (2013) 14–19.
[18] S.J. Yang, T. Kim, J. HyukIm, Y.S. Kim, K. Lee, H. Jung, C.R. Park, Chem. Mater. 24 (2012) 464–470.
[19] B. Panella, M. Hirscher, H. Putter, U. Muller, Adv. Funct. Mater. 16 (2006) 520.
[20] J. Li, B. Peng, G. Zhou, Z.A. Zhang, Y.Q. Lai, M. Jia, ECS Electrochem. Lett. 2 (2013) A25–A27.
[21] N. Jayaprakash, J. Shen, S.S. Moganty, A. Corona, L.A. Archer, Angew. Chem. Int. Ed. 50 (2011) 5904–5908.
[22] X.L. Ji, S. Evers, R. Black, L.F. Nazar, Nat. Commun. 2 (2011) 325.
[23] J.W. Choi, G. Cheruvally, D.S. Kim, J.H. Ahn, K.W. Kim, H.J. Ahn, J. Power Sources 183 (2008) 441.
[24] Z.F. Deng, Z.A. Zhang, Y.Q. Lai, J. Liu, J. Li, Y.X. Liu, J. Electrochem. Soc. 160 160 (2013) A553–A558.